ELSEVIER

Journal of Structural Geology 26 (2004) 1773–1781

JOURNAL OF STRUCTURAL GEOLOGY

www.elsevier.com/locate/jsg

Extensional detachment at the inclusion–matrix interface in a multiple inclusion system

Nibir Mandal[a], Gautam Bhattacharyya[a], Chandan Chakraborty[b,*]

[a]*Department of Geological Sciences, Jadavpur University, Kolkata 700032, India*
[b]*Geological Studies Unit, Indian Statistical Institute, 203, B.T. Road, Kolkata 700108, India*

Received 2 May 2003; received in revised form 5 January 2004; accepted 10 January 2004

Available online 14 May 2004

Abstract

This paper deals with a theoretical analysis of extensional fissures around spherical rigid inclusions hosted in a ductile matrix undergoing bulk shear. The analysis shows that the mechanical interaction of inclusions is a function of the inclusion concentration a/b ($2a$ and $2b$ are the inclusion diameter and mean inter-inclusion distance, respectively), and intensifies the tensile stress imparted by the flowing matrix on the inclusion–matrix interface. Inclusion concentration a/b thus appears to be a crucial parameter in perturbing the inclusion–matrix coherence and leading to formation of extensional fissures around an inclusion. We performed numerical simulations to delineate the fields for coherent and incoherent interfaces in the $T_o^* - a/b$ space, where T_o^* is the tensile strength of the interface, normalized to $\eta\dot{\gamma}$, where η and $\dot{\gamma}$ are the viscosity of matrix and bulk shear rate, respectively. For a given a/b, the interface cannot remain coherent unless the tensile strength is greater than a critical value. The critical T_o^* increases almost linearly at a gentle gradient with increasing a/b. However, for $a/b > 0.7$, this increases nonlinearly, assuming a large value when the concentration is high ($a/b > 0.8$). It is also revealed that under the same deformation conditions, the instantaneous opening in fissures may vary depending upon the a/b values.

Keywords: Inclusion–matrix systems; Fissures; Tensile strength; Interaction and stress field

1. Introduction

Many rocks contain stiff inclusions (e.g. porphyroclasts, porphyroblasts, etc.) floating in a ductile matrix. During deformation, the inclusions mechanically interact with one another when they occur in large volume proportions in the rock. Theoretical and experimental studies demonstrate that such mutual interaction affects the rotational kinematics of inclusions, the matrix flow around them (Shimammoto, 1975; Ildefonse et al., 1992; Treagus, 2002; Samanta et al., 2003), and their internal strain when they are deformable (Mandal et al., 2003). It appears from these studies that traction at inclusion–matrix interfaces will depend upon the interaction, which is a function of inclusion concentration. In this paper we investigate how the mechanical interaction among rigid inclusions modifies the traction at the inclusion–matrix interface and, in turn, may affect the coherence between inclusion and matrix, which is a crucial physical condition considered in different analyses on inclusion–matrix rock systems (Ildefonse and Mancktelow, 1993; Marques and Cobbold, 1995; Kenkmann and Dresen, 1998; Pennacchioni et al., 2000; Ramsay and Lisle, 2000; Marques and Coelho, 2001; Mancktelow et al., 2002).

Observations on naturally deformed inclusion–matrix rock systems indicate that the inclusion–matrix coherence may be locally affected, and there may be detachment of matrix from the inclusion, forming fissures on either side of the inclusions (Ramsay and Huber, 1983). These fissures are generally filled with crystal fibers. Their growth patterns, e.g. face controlled and displacement controlled, are guided by the detachment kinematics (Ramsay and Huber, 1983; Urai et al., 1991). In order to study the mechanics of these extensional fissures, it is primarily necessary to understand the physical factors that trigger coherence to incoherence transition at the inclusion–matrix interface. Recent studies reveal that the shape and orientation of the inclusion control the detachment at the inclusion–matrix interfaces (Samanta

* Corresponding author.
E-mail address: chandan@isical.ac.in (C. Chakraborty).

0191-8141/$ - see front matter © 2004 Published by Elsevier Ltd.
doi:10.1016/j.jsg.2004.01.011

and Bhattacharyya, 2003). The analyses, however, deal with single rigid inclusions floating in an infinite ductile matrix, and are thus applicable to rocks containing inclusions in low volume concentrations. Interacting inclusions experience matrix-traction different from that of single, non-interacting inclusions (Samanta et al., 2003), and the conditions for inclusion–matrix detachment in such cases are different, calling for a separate analysis.

In this paper we present a theoretical analysis to show the effect of mechanical interaction on the stability of inclusion–matrix interfaces in a system of rigid spherical inclusions in a viscous matrix, and demonstrate how the inclusion concentration can influence the formation of extensional fissures at the inclusion–matrix interface in bulk simple shear deformation. This analysis involves the velocity functions for flow outside an interacting spherical inclusion in a viscous matrix (Happel, 1957; Samanta et al., 2003). Theoretical results are complemented with findings from physical model experiments.

2. Theoretical consideration

2.1. Mathematical derivations

Consider a coherent inclusion–matrix system consisting of rigid spherical inclusions of diameter $2a$ with a mean inter-inclusion distance $2b$ within a Newtonian viscous matrix (Fig. 1a). The system is deformed under bulk simple shear at a rate $\dot{\gamma}$. A Cartesian reference, xyz, is chosen at the center of an inclusion with x axis oriented parallel to the shear direction and z axis oriented along the direction of no bulk flow (Fig. 1b). The bulk shear $\dot{\gamma}$ can be resolved into distortion (e_{xy}) and rotation (ζ) parts, where $e_{xy} = \dot{\gamma}/2$ and $\zeta = \dot{\gamma}/2$. For a homogeneous flow, i.e. in the absence of inclusions, the velocity components corresponding to e_{xy} and ζ can be written in terms of the Cartesian coordinates, respectively, as:

$$u_D^* = \frac{\dot{\gamma}}{2}y; \qquad v_D^* = \frac{\dot{\gamma}}{2}x; \qquad w_D^* = 0 \tag{1a}$$

$$u_R^* = \frac{\dot{\gamma}}{2}y; \qquad v_R^* = -\frac{\dot{\gamma}}{2}x; \qquad w_R^* = 0 \tag{1b}$$

The flow perturbations due to the presence of inclusions need to be determined separately for distortion (e_{xy}) and rotation (ζ) parts, which can be combined with Eqs. (1a) and (1b) to obtain the entire flow field around an inclusion.

Using Lamb's (1932) theory of spherical harmonics for hydrodynamics, Happel (1957) presented flow perturbations around an inclusion as a function of inter-inclusion spacing for the distortion part e_{xy} of bulk shear. Their expressions in

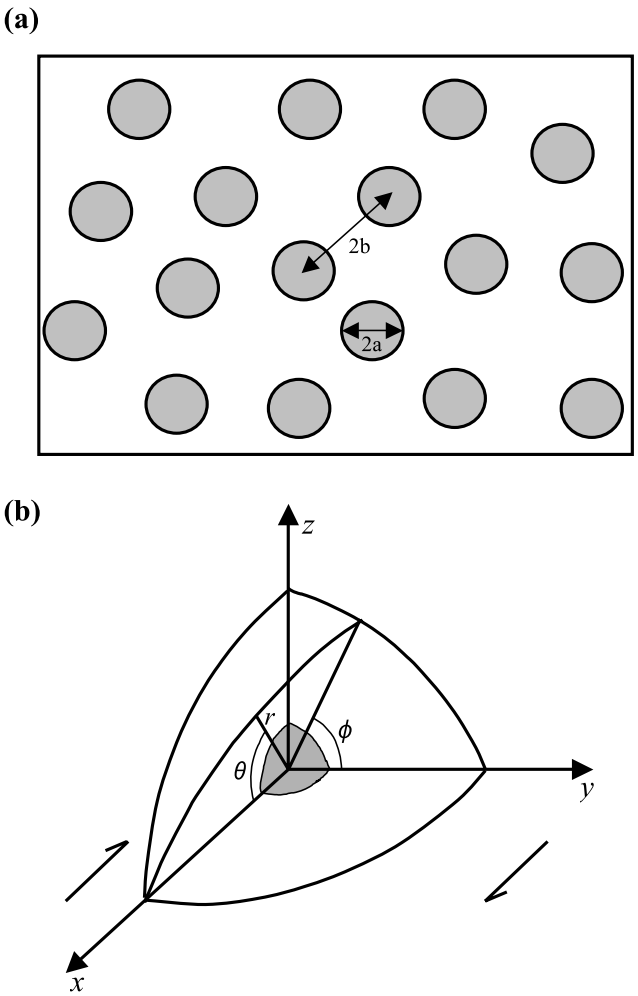

Fig. 1. (a) Consideration of inclusion–matrix system for theoretical analysis. (b) Choice of spherical co-ordinate frame at the center of an inclusion.

spherical coordinates follow:

$$\begin{aligned} v_r &= \left[6r^3A + 2rB + \frac{6}{r^2}C - \frac{3D}{r^4}\right]\dot{\gamma}\cos\phi\sin\theta\cos\theta \\ v_\theta &= \left[5r^3A + rB + \frac{D}{r^4}\right]\dot{\gamma}\cos\phi(\cos^2\theta - \sin^2\theta) \\ v_\phi &= -\left[5r^3A + rB + \frac{D}{r^4}\right]\dot{\gamma}\sin\phi\cos\theta \end{aligned} \tag{2}$$

v_r, v_θ and v_ϕ are the velocity components in the direction of positive r, θ and ϕ, respectively (Fig. 1b). Samanta et al. (2003) have considered mutual rotational interaction among rigid inclusions in the system, and derived the flow perturbation around a rigid inclusion corresponding to the rotational part ζ. This perturbation is added to that in Eq. (2), and then taking Eqs. (1a) and (1b) in spherical coordinates,

the total flow field can be expressed as:

$$v_r = \left[6r^3A + 2rB + \frac{6}{r^2}C - \frac{3D}{r^4} + r\right]\dot{\gamma}\cos\phi\sin\theta\cos\theta$$

$$v_\theta = \left[\left(5r^3A + rB + \frac{D}{r^4} + \frac{r}{2}\right)\left(\cos^2\theta - \sin^2\theta\right) - \frac{1}{2}\left(r - \frac{a^6}{b^3r^2}\right)\right]\dot{\gamma}\cos\phi$$

$$v_\phi = -\left[5r^3A + rB + \frac{D}{r^4} + \frac{1}{2}\frac{a^6}{b^3r^2}\right]\dot{\gamma}\sin\phi\cos\theta \qquad (3)$$

where A, B, C and D are constants, and their expressions are:

$$A = -\frac{5}{2a^2}\left(\frac{\alpha^7}{10+4\alpha^7}\right)\beta,$$

$$B = \frac{5}{4}\left(\frac{4+10\alpha^7}{10+4\alpha^7}\right)\beta - \frac{1}{2}, \qquad C = -\frac{5a^3}{12}\beta, \qquad (4)$$

$$D = -\frac{5a^5}{10+4\alpha^7}\beta$$

where

$$\beta = \frac{10+4\alpha^7}{10(1-\alpha^{10}) - 25\alpha^3(1-\alpha^4)}$$

and $\alpha = a/b$.

The constants are functions of the a/b ratio (Eq. (4)), which can be considered as a measure of volume concentration of rigid inclusions in the system. The ratio may vary from zero to one, representing, respectively, a very dilute suspension, comparable with single inclusion systems and an extremely dense suspension, where the inclusions are in contact with one another.

With the help of the velocity functions in Eq. (3) we can now determine the stress at any point in the flowing matrix. In spherical coordinates the relations between the stress and the velocity gradient tensors are:

$$\sigma_{r\theta} = \eta\left[\frac{1}{r}\frac{\partial v_r}{\partial\theta} + \frac{\partial v_\theta}{\partial r} - \frac{v_\theta}{r}\right],$$

$$\sigma_{r\phi} = \eta\left[\frac{1}{r\sin\theta}\frac{\partial v_r}{\partial\phi} + \frac{\partial v_\phi}{\partial r} - \frac{v_\phi}{r}\right],$$

$$\sigma_{\theta\phi} = \eta\left[\frac{\sin\theta}{r}\frac{\partial}{\partial\theta}\left(\frac{v_\phi}{\sin\theta}\right) + \frac{1}{r\sin\theta}\frac{\partial v_\theta}{\partial\phi}\right],$$

and

$$\sigma_{rr} = \left[-p + 2\eta\frac{\partial v_r}{\partial r}\right],$$

$$\sigma_{\theta\theta} = \left[-p + 2\eta\left\{\frac{1}{r}\frac{\partial v_\theta}{\partial\theta} + \frac{v_r}{r}\right\}\right], \qquad (5)$$

$$\sigma_{\phi\phi} = \left[-p + 2\eta\left\{\frac{1}{r\sin\theta}\frac{\partial v_\phi}{\partial\phi} + \frac{v_r}{r} + \frac{v_\theta\cot\theta}{r}\right\}\right]$$

where p and η are the confining pressure and the viscosity of matrix, respectively. After Happel (1957) we find the expression of p:

$$p = \eta\left(42r^2A + 12\frac{C}{r^3}\right)\cos\phi\sin\theta\cos\theta \qquad (6)$$

Substituting the expressions of v_r, v_θ, v_ϕ (Eq. (3)) and p (Eq. (6)) in Eq. (5), we get:

$$\sigma_{rr} = (-6r^2A + 4B - 36\frac{C}{r^3} + 24\frac{D}{r^5} + 2)\eta\dot{\gamma}\cos\phi\sin\theta\cos\theta$$

$$\sigma_{\theta\theta} = \left[-70r^2A - 4B - 14\frac{D}{r^5} - 2\right]\eta\dot{\gamma}cos\phi\sin\theta\cos\theta$$

$$\sigma_{\phi\phi} = \left[-50r^2A - 10\frac{D}{r^5}\right]\eta\dot{\gamma}\cos\phi\sin\theta\cos\theta$$

$$\sigma_{r\theta} = \left[\left(16r^2A + 2B + 6\frac{C}{r^3} - 8\frac{D}{r^5} + 1\right) \times\cos2\theta - \frac{3}{2}\frac{a^6}{b^3r^3}\right]\eta\dot{\gamma}\cos\phi$$

$$\sigma_{r\phi} = -\left[16r^2A + 2B + 6\frac{C}{r^3} - 8\frac{D}{r^5} + 1 - \frac{3}{2}\frac{a^6}{b^3r^3}\right]\eta\dot{\gamma}\sin\phi\cos\theta$$

$$\sigma_{\theta\phi} = 2\left[5r^2A + B + \frac{D}{r^5} + \frac{1}{2}\right]\eta\dot{\gamma}\sin\theta\sin\phi \qquad (7)$$

2.2. Analysis of stress at the inclusion–matrix interface

Using Eq. (7), we can determine the traction at different points on the inclusion–matrix interfaces considering the effect of inclusion concentration. We performed the analysis on a two-dimensional section perpendicular to the direction of no bulk flow (i.e. z axis), passing through the center of the inclusion. After substituting $r = a$ in Eq. (5), the normal and shear components of the traction can be shown as a function of θ for a given value of the a/b ratio (Figs. 2 and 3). For convenience, the radial and tangential stress components are normalized as:

$$\sigma^*_{rr} = \frac{\sigma_{rr}}{\eta\dot{\gamma}}$$

and

$$\sigma^*_{r\theta} = \frac{\sigma_{r\theta}}{\eta\dot{\gamma}}$$

We then analyze their variations along the inclusion–matrix interface (i.e. with θ). The normal stress is tensile in the range of $0 > \theta < 90°$, with a peak at $\theta = 45°$ (Fig. 2). The maximum value of the tensile stress is sensitive to the a/b ratio. This is less than 25 when a/b is less than 0.6. However, the stress exceeds 100 when a/b is greater than 0.8. This implies that the mutual mechanical interaction resulting from larger concentrations of inclusions in the system leads to stress intensification at the inclusion–matrix

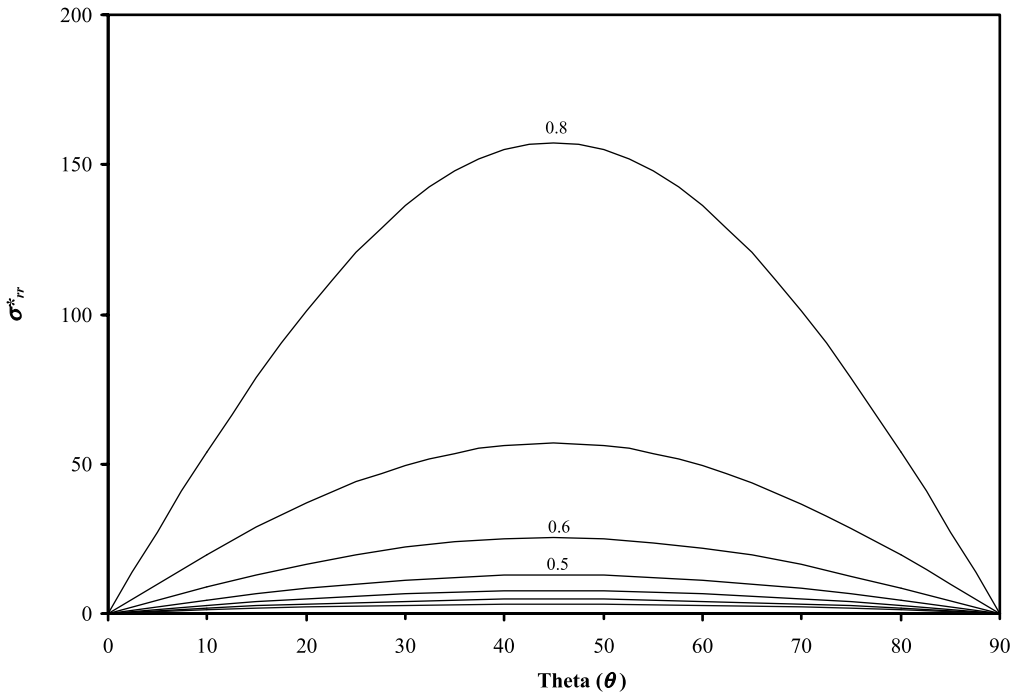

Fig. 2. Calculated plots showing variations of the normalized tensile stress σ^*_{rr} ($= \sigma_{rr}/\eta\dot{\gamma}$) at the inclusion–matrix interface with θ for different inclusion concentrations (*a*/*b*).

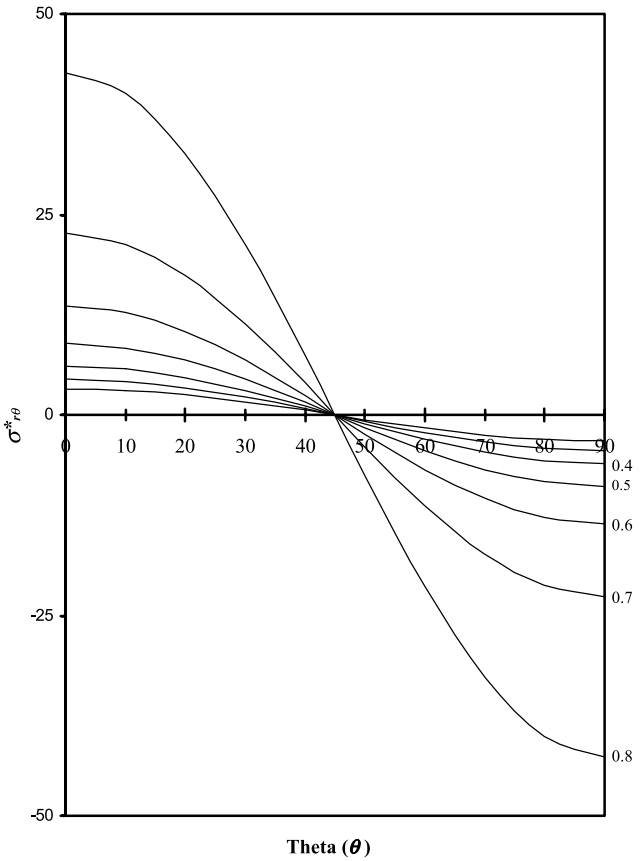

Fig. 3. Variations of shear stresses $\sigma^*_{r\theta}$ ($= \sigma_{r\theta}/\eta\dot{\gamma}$) at the inclusion–matrix interface for different inclusion concentrations (*a*/*b*).

interfaces. Similarly, the shear stress component, normalized to the bulk flow stress, varies systematically with θ, and the variation also depends on the *a*/*b* ratio (Fig. 3). For a given *a*/*b* value, the shear stress is a maximum at $\theta = 0$, and then decreases down to zero at $\theta = 45°$, and the sense of shear stress reverses with further increase in θ, showing a minimum at $\theta = 90°$. It is found from the plots that the inclusion concentration, i.e. *a*/*b* ratio, has a greater effect in intensifying the normal stress component, relative to the shear stress component. When the *a*/*b* ratio is 0.8, the maximum value of normalized tensile stresses becomes more than 100, whereas that of normalized shear stresses remains less than 50.

In response to the traction, the inclusion–matrix interface may experience extensional detachment at places where the tensile stress exceeds the tensile strength of the interface. Since increasing inclusion concentration appears to intensify the normal traction, this may be an important parameter facilitating development of extensional fissures around inclusions in a multiple inclusion system, as revealed in the numerical simulations presented below.

2.3. Numerical simulations of extensional fissures

A computer program was developed in Visual Basic to compute the tensile stress component acting on the surface of the inclusion, and to find points on the inclusion where the tensile stress exceeds the tensile strength (T_o) of the inclusion–matrix interface The strength was normalized to $\eta\dot{\gamma}$, which is denoted hereafter as T^*_o. Instantaneous

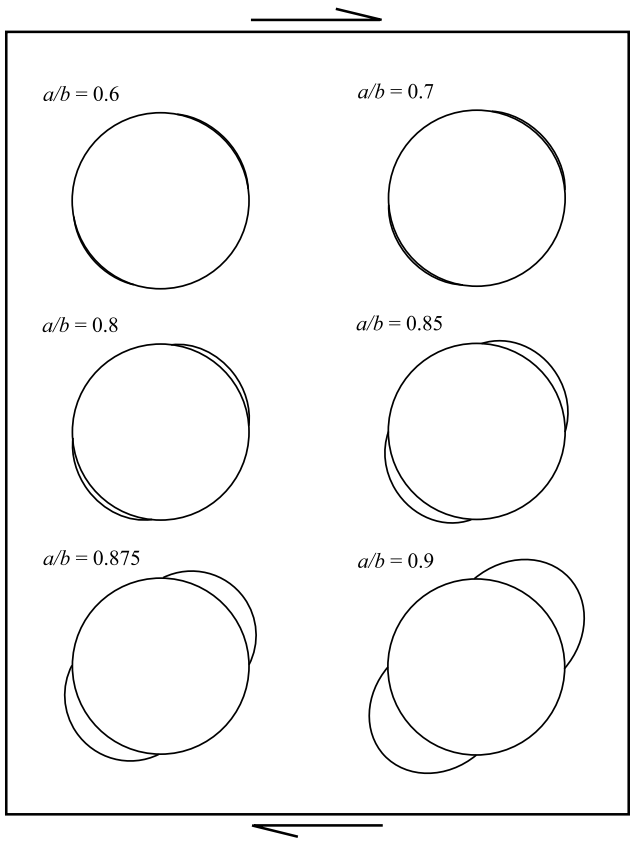

Fig. 4. Numerical simulations of instantaneous extensional fissures adjacent to circular inclusions under bulk simple shear. Note that the degree of opening increases with increasing inclusion concentration *a/b*.

displacements of these points following detachment were then computed to delineate the fissure, considering a direct proportionality between displacement and normal traction (cf. Samanta and Bhattacharyya, 2003; also see discussion). Using Eq. (7) we performed a set of numerical experiments by varying the inclusion concentration parameter *a/b* (Fig. 4). Numerical models reveal that for the imposed value of tensile strength ($T_o^* = 1$) inclusions do not develop perceptible fissures at their interface with the matrix, when *a/b* is less than 0.5. For the same tensile strength, when the ratio is larger than 0.6, detachment occurs at the inclusion–matrix interface giving rise to symmetrical fissures on either side of the inclusion with maximum opening oriented at an angle of 45° with the shear direction. The magnitude of maximum opening is also found to be sensitive to the *a/b* ratio, and increases steeply when *a/b* is larger than 0.7. With increase in *a/b*, detachment occurs over large arc-lengths of the inclusion–matrix interface. However, fissure opening normal to the wall is much more sensitive to the *a/b* ratio, compared with its lateral increment.

2.4. Stability field of inclusion–matrix interface

The stability of inclusion–matrix interfaces will depend on two factors: inherent tensile strength of the interface and stress resulting from the flowing matrix in an interacting state In the previous section we have seen that the stress is a function of inclusion concentration. Thus, the fields defining the conditions for coherent and incoherent interfaces can be shown in terms of its normalized tensile strength T_o^* and inclusion concentration (*a/b*) (Fig. 5). For a given T_o^*, the *a/b* ratio shows a critical value where the maximum tensile stress at the interface tends to exceed the tensile strength and thereby the coherent interface becomes incoherent. For example, if $T_o^* = 10$, the interface will become incoherent, developing fissures when *a/b* exceeds 0.72 (Fig. 5).

With the help of Eq. (5) we calculated the critical tensile strength (T_o^*), i.e. the strength required for maintaining interfaces intact, as a function of inclusion concentration (*a/b*), and defined the fields for inclusions with coherent and incoherent interfaces. The plot (Fig. 5) shows that the critical T_o varies more or less linearly at a gentle gradient with the *a/b* ratio when $a/b < 0.7$, defining a narrow field for the formation of extensional fissures. For very low inclusion concentrations ($a/b < 0.1$) fissures can develop only when the normalized tensile strength of the interface is less than 2.5. With increase in inclusion concentration this increases to about 10 when $a/b = 0.7$. For larger *a/b*, the critical T_o^* increases nonlinearly with *a/b*, assuming a steep gradient when $a/b > 0.8$. Thus, the field for inclusions with incoherent interfaces widens with *a/b*, and the tensile strength required for maintaining a coherent interface becomes very large (Fig. 5). The analysis implies that increasing inclusion concentration promotes formation of extensional fissures in inclusion–matrix systems.

3. Experimental verification

We carried out a set of simple, analog experiments to test the analytical results described in the previous sections. Interacting inclusion–matrix systems were simulated by embedding a number of short, circular cylindrical rigid objects within a block of commercial putty (viscosity in the order of 10^4 Pa s) (Fig. 6). There was an isolated object in the putty block, which behaved as a single object in the matrix. The model was deformed in simple shear at a rate of 1.5×10^{-3}/s. A set of experiments was run by varying the concentration of objects, i.e. the *a/b* ratio.

In all the experiments the isolated objects maintained a coherent interface with the matrix, and thus did not produce fissures at any stage of progressive shear deformation. On the other hand, the interfaces of objects occurring in multiple associations showed contrasting responses, depending upon their concentration in the matrix (Fig. 7). In experiments with a low object concentration the object–matrix interfaces remained coherent, as in the isolated object (Fig. 7a). Under the same strain, whereas the isolated object had an intact interface, multiple objects in larger concentrations showed incoherent interface, developing

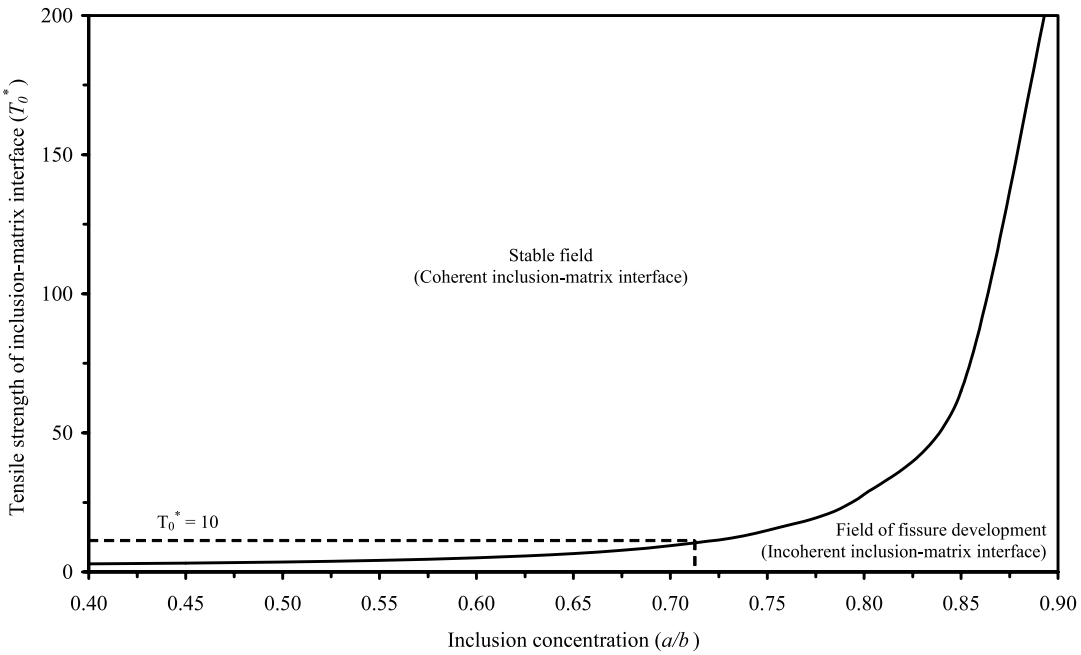

Fig. 5. Fields for inclusions with coherent and incoherent interfaces in $T_o^* - a/b$ space. T_o^* is the tensile strength of interface normalized to $\eta\dot{\gamma}$. Dashed lines show an example of critical a/b corresponding to a given tensile strength. For $T_o^* = 10$, a coherent interface will become incoherent if $a/b > 0.71$.

fissures on either side of each object (Fig. 7b). The opening of fissures was found to be a function of the concentration of objects in the model, as revealed from the numerical simulations (Fig. 4). With increase in object concentration the detachment occurred rapidly, forming fissures with large opening for the same amount of bulk shear (Fig. 7b and c).

The experimental findings reveal two principal facts: (1) the mechanical stability of inclusion–matrix interface decreases, resulting in coherence to incoherence transition with increasing inclusion concentration and (2) the magnitude of opening of fissure is larger for larger inclusion concentration in the matrix.

4. Discussion

Our study primarily aims at analyzing the role of inclusion concentration on inclusion–matrix coherence, a crucial physical factor in rock composites, such as conglomerates, mylonites and augen gneisses. We consider some examples to discuss its geological implications. In many metamorphic rocks large, rigid mineral grains are associated with crystal fibers, which are found to be useful kinematic indicators (Ramsay and Huber, 1983). The most fundamental step in explaining these structures needs an understanding of the conditions triggering detachment of the matrix from mineral grains. Our analysis suggests that rigid grains occurring in high concentration are more likely to develop fissure-controlled fibers, as their interfaces are prone to extensional detachment. The degree of inclusion–matrix coherence again affects the strain field around rigid inclusions (Ildefonse and Mancktelow, 1993; Pennacchioni et al., 2000). It appears from this analysis that increasing inclusion concentration facilitates inclusion–matrix detachment, and thereby can modify the heterogeneous strain distribution around the inclusion. Thus, under the same bulk

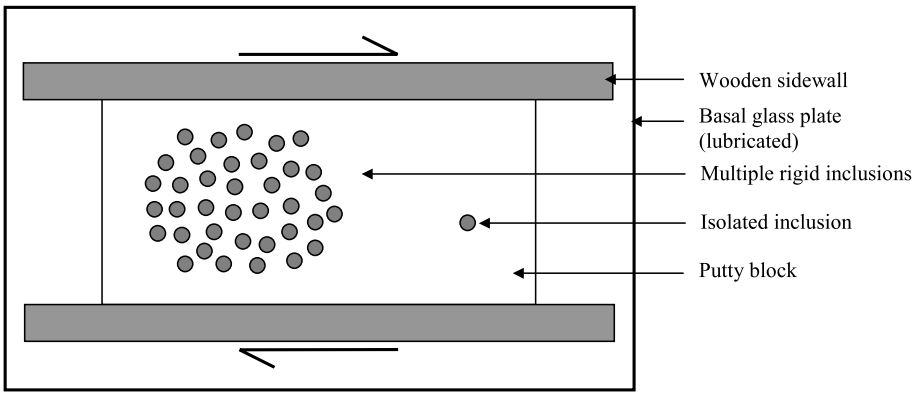

Fig. 6. A schematic sketch of the experimental setup. The model consisted of rigid inclusions floating in a ductile matrix of commercial putty.

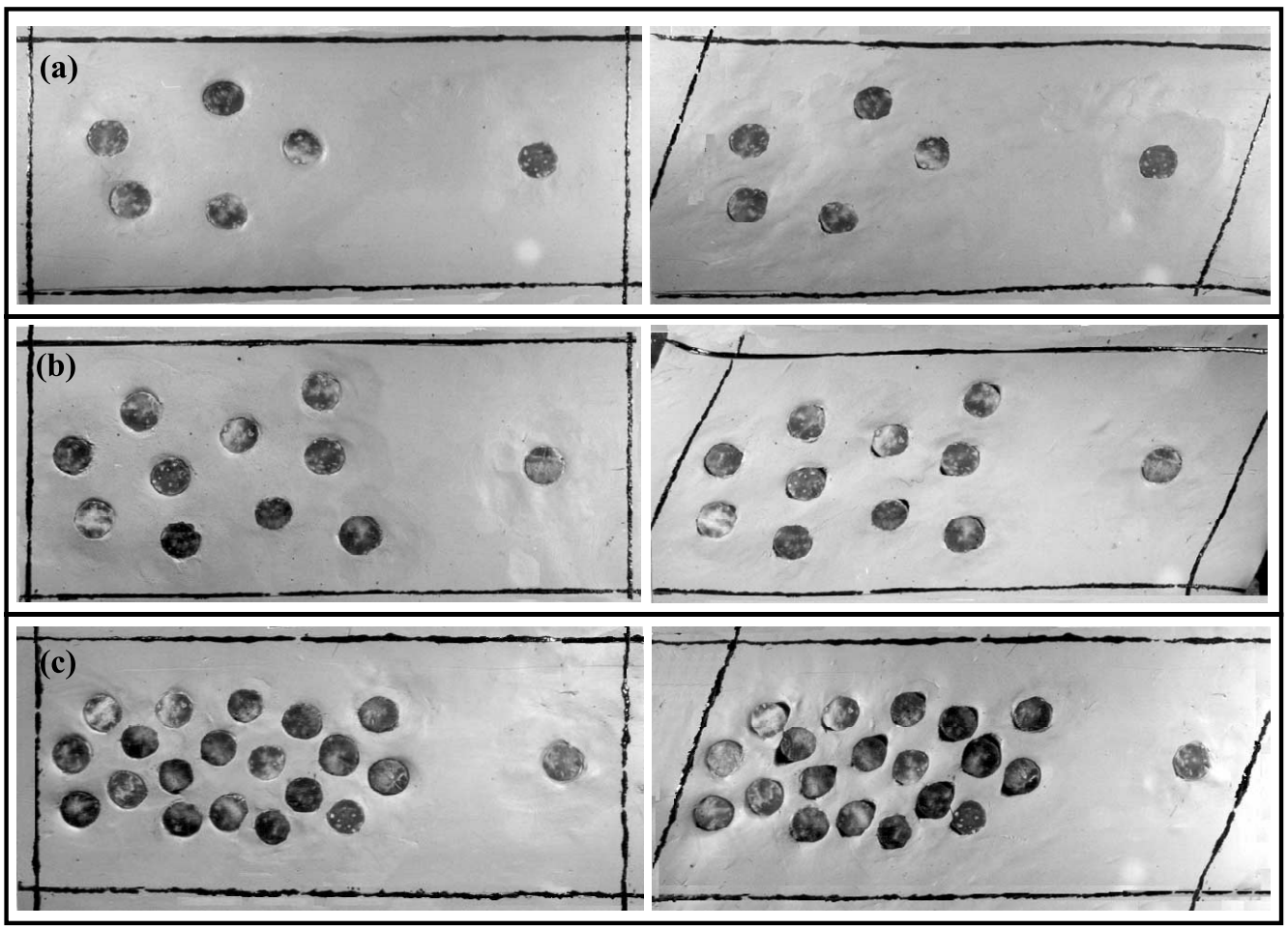

Fig. 7. Initial (left) and deformed (right) physical models. The models were deformed to about the same amount of bulk shear ($\gamma = 0.18$). Note that the isolated inclusions did not develop detachment in any of the experiments. $a/b = 0.4$, 0.5 and 0.7 in (a), (b) and (c), respectively. Scale: inclusion diameter = 1 cm.

kinematics structures, e.g. foliation drag, porphyroclast tails, developing under the influence of heterogeneous strain field around large grains may be different in different locales depending on the variation in their initial concentration in the rock.

The analysis shows that the magnitude of tensile stress at the inclusion–matrix interface increases non-linearly with increasing inclusion concentration (Fig. 2), and assumes a large value when the concentration is greater than 0.8. Thus, inclusions occurring in high concentrations can undergo detachment from the matrix over a large area of their interface if the cohesional strength is not high. In such a condition fissures can form encompassing almost the entire portion of the inclusion–matrix interface lying in the extensional field. This type of extensional fissures is sometimes observed around stiff objects, e.g. ooids, in naturally deformed rocks (cf. figs. 7.7 and 7.8 of Ramsay and Huber, 1983).

We ran numerical simulations based on several considerations, which need to be addressed. Numerical models are idealized with statistically random distribution of spherical rigid inclusions, where the boundary conditions defining the inter-inclusion interaction are imposed on the surface of a co-centric spherical shell with the radius equal to the mean inter-inclusion distance. It is assumed that the same interaction condition prevails over the entire surface of the shell, where the positional distributions of the neighboring inclusions are not taken into account. Under this consideration the direction of maximum tensile stress is always oriented at an angle of 45° to the shear direction, irrespective of volume concentration. This is evidently a statistical orientation, and agrees with our findings in physical experiments. However, there may be departures due to variation in the distance of neighboring inclusions. For example, the direction of maximum tensile stress may get tilted towards a neighboring inclusion located very close to the inclusion under consideration. Considering random dispositions of the neighboring inclusions, the average orientation of maximum tensile stress should be at an angle of 45° to the shear direction, as revealed from the theoretical analysis.

The mathematical derivations in the theoretical analysis are applicable for small amounts of deformation, i.e. as long as the boundary conditions on the spherical shell remain valid. Again, the derivation of stresses at the inclusion–matrix interface involves velocity functions for flow of

matrix, which is based on coherent condition of inclusion and matrix. The functions will not remain valid as soon as incoherence develops at the inclusion–matrix interface. In the numerical simulations we have shown fissures developing at the instant of coherent to incoherent transition. They actually represent varying rates of opening due to varying inclusion concentrations. Evidently, the theoretical approach is not tenable to decipher the progressive development of fissures in the course of deformation. The simulations involve exaggeration of the magnitude of instantaneous opening and demonstrate how increasing volume concentration promotes fissure generation. The magnitude of opening at the moment of detachment is assumed to be directly proportional to the tensile stress acting at the inclusion–matrix interface. This is a somewhat simplistic assumption, which we can correlate with that obtained analytically from the plane theory of elasticity. The analytical solutions (eqs. 58.9 and 58.10 of Muskhelishvilli, 1953) show that the displacement components at the interface of the incoherent circular rigid object are linear functions of the stress components at that point. In our numerical simulations we have chosen the proportionality factor arbitrarily in such a manner that the differences in fissure opening due to varying inclusion concentrations become obvious. It is likely that fissure geometry shown in the numerical models will undergo modifications with progressive deformation, as their boundary will subsequently get distorted in response to the heterogeneous strain field around the inclusion. The finite opening of fissures will also depend on the displacement of neighboring inclusions, which is a function of finite bulk strain. Thus, the final geometry of fissures will be different from those shown in numerical models.

In the analysis of inclusion–matrix detachment we intentionally avoid using any failure criterion, as the surface of detachment is a contact between a rigid solid and a ductile material. Detachment occurs preferentially along the interface, which is not exactly similar to rupturing in a continuous, brittle medium. We have used tensile strength, which is the stress required to break the adherence between the two contrasting materials. In natural conditions other physical factors, e.g. pressure solution, formation of new mineral phases defining a film at the inclusion–matrix interface, can control the mechanical condition at the interface and thereby formation of fissures in the neighborhood of an inclusion.

Experimental findings grossly conform to the results obtained from theoretical analyses. However, the results cannot be compared quantitatively. For example, increasing inclusion concentration promotes formation of extensional fissures both in theoretical and experimental models. But, both the magnitude and geometry of fissures show some dissimilarities. These differences are due to simplistic considerations in numerical simulations. The opening in numerical models represent an instantaneous event at the moment of detachment, where its magnitude is considered to be proportional to the tensile stress with an arbitrary scale factor, which is not constrained with experimental conditions. Secondly, their geometry actually represents the configuration of the fissure at the very initial stage, and this cannot be compared with the tapered fissures in physical experiments, which has developed through modification in the course of progressive deformation. In addition, the mechanical conditions at the inclusion–matrix interface could not be maintained perfectly uniform while preparing an experimental model. This variation resulted in non-uniform development of fissures along the inclusion–matrix interface in experimental models. The differences cited above may also occur due to the difference in matrix rheology. In theory the matrix is considered to be Newtonian. On the other hand, the rheology of putty that we used as the matrix material in physical experiments is not well constrained. However, it appears to be non-Newtonian. There was also a difference in three-dimensional geometry of rigid inclusions considered in theory and experiments. In theory the inclusion are ideally spherical, whereas in experiments, for convenience, short cylindrical inclusions were used. It appears, however, that the central section of a spherical inclusion is nearly equivalent to a section orthogonal to the long axis of short cylindrical inclusions. In spite of all these limitations the experiments are complementary to our principal findings that under the same conditions, increasing the inclusion concentration leads to detachment at the inclusion–matrix interface, and thereby facilitates formation of fissures in the neighborhood of an inclusion.

The development of fissures in the neighborhood of rigid objects involves volume adjustment. In natural conditions opening of fissures is simultaneously filled with diffusive minerals, such as quartz or calcite. Thus, positive volume changes due to formation of fissures can be balanced by negative volume changes in the matrix, and the bulk deformation may take place under constant-volume conditions. In our experiments the volume adjustment probably took place through development of surface relief. Theoretical analysis presented in this paper does not take into account this type of complex mechanisms required for volume adjustment. The analysis only explains how instantaneous separation can take place in response to the stresses at the inclusion–matrix interface without considering how the volume generated due to opening is counter-balanced. Further studies are required to investigate the modes of volume adjustment around rigid inclusions.

There are some other limitations in the study, which, however, do not hinder our main proposition on the effect of inclusion concentration in inclusion–matrix systems. The analysis is presented considering the effective bulk flow stress. Evidently, confining pressure will be an additional parameter in determining the effective traction and thereby formation of fissures at the inclusion–matrix interfaces.

5. Conclusions

The principal outcomes of our analysis are concluded along the following points:

1. In multiple inclusion systems the mechanical interaction of inclusions influences the inclusion–matrix coherence.
2. The tensile stress at the inclusion–matrix interface is a non-linear function of inclusion concentration a/b. With increase in a/b the stress assumes a large value when $a/b > 0.8$.
3. Mechanical interaction promotes formation of extensional fissures on either side of individual inclusions. The instantaneous opening in the fissures is larger for larger inclusion concentrations.
4. Inclusion–matrix interfaces can remain coherent if their tensile strength is larger than a critical value, which is a function of inclusion concentration a/b. For inclusion concentration $a/b < 0.7$, the critical tensile strength increases linearly at a gentle gradient with a/b, whereas this increases non-linearly with steep gradients when $a/b > 0.7$.

Acknowledgements

We thank Professors S.H. Treagus, F.O. Marques and R. Taborda for their critical reviews, which have greatly improved the manuscript. We are grateful to Professor J. Hippertt for giving us an outline for revising the manuscript. NM and GB wish to thank the DST and the CSIR of India, respectively, for providing support in carrying out this work. CC acknowledges infrastructural facilities provided by the Indian Statistical Institute, Calcutta.

References

Happel, J., 1957. Viscosity of suspensions of uniform spheres. Journal of Applied Physics 28, 1288–1292.

Ildefonse, B., Mancktelow, N.S., 1993. Deformation around rigid particle: influence of slip at the particle/matrix interface. Tectonophysics 221, 345–359.

Ildefonse, B., Sokoutis, D., Mancktelow, N.S., 1992. Mechanical interactions between rigid particles in a deforming ductile matrix. Analogue experiments in simple shear flow. Journal of Structural Geology 14, 1253–1266.

Kenkmann, T., Dresen, G., 1998. Stress gradients around porphyroclasts: palaeo-piezometric estimates and numerical modeling. Journal of Structural Geology 20, 163–173.

Lamb, H., 1932. Hydrodynamics, Cambridge University Press, Cambridge.

Mancktelow, N.S., Arbaret, L., Pennacchioni, G., 2002. Experimental observations on the effect of interface slip on rotation and stabilisation of rigid particles in simple shear and a comparison with natural mylonites. Journal of Structural Geology 24, 567–585.

Mandal, N., Samanta, S.K., Bhattacharyya, G., Chakraborty, C., 2003. Deformation of ductile inclusions in a multiple inclusion system in pure shear. Journal of Structural Geology 25, 1359–1370.

Marques, F.O., Cobbold, P.R., 1995. Development of highly non-cylindrical folds around rigid ellipsoidal inclusions in bulk simple shear: natural examples and experimental modelling. Journal of Structural Geology 17, 589–602.

Marques, F.O., Coelho, S., 2001. Rotation of rigid elliptical cylinders in viscous simple shear flow: analogue experiments. Journal of Structural Geology 23, 609–617.

Muskhelishvilli, N.I., 1953. Some Basic Problems of Mathematical Theory of Elasticity, Noordhoff, Groningen, 704pp.

Pennacchioni, G.P., Fasolo, L., Cecchi, M.M., Salasnich, L., 2000. Finite-element modeling of simple shear flow in Newtonian and non-Newtonian fluids around circular rigid particle. Journal of Structural Geology 22, 683–692.

Ramsay, J.G., Huber, M.I., 1983. The Techniques of Modern Structural Geology. Volume 1: Strain Analysis, Academic Press, London.

Ramsay, J.G., Lisle, R.J., 2000. The Techniques of Modern Structural Geology. Volume 3: Continuum Mechanics in Structural Geology, Academic Press, London.

Samanta, S.K., Bhattacharyya, G., 2003. Modes of detachment at the inclusion–matrix interface. Journal of Structural Geology 25, 1107–1120.

Samanta, S.K., Mandal, N., Chakraborty, C., 2003. Flow patterns around mechanically interacting rigid inclusions under simple shear: theoretical model and geological implications. Journal of Structural Geology 25, 209–221.

Shimammoto, T., 1975. The finite element analysis of the deformation of a viscous spherical body embedded in a viscous medium. Journal of the Geological Society of Japan 81, 255–267.

Treagus, S.H., 2002. Modelling the bulk viscosity of two-phase mixtures in terms of clast shape. Journal of Structural Geology 24, 57–76.

Urai, J.L., Williams, P.F., Van Roermund, H.L.M., 1991. Kinematics of crystal growth in syntectonic fibrous veins. Journal of Structural Geology 13, 823–836.